Chemical Engineering Journal 534 (2026) 175093

Contents lists available at ScienceDirect

Chemical Engineering Journal

journal homepage: www.elsevier.com/locate/cej

Critical bistability in variable cross-section metamaterials: PINN-driven transient stress recognition and adaptive energy dissipation

Jian Zhou [a], Chengjun Zeng [a], Wei Zhao [a,*], Jinsong Leng [b], Yanju Liu [a,*]

[a] Department of Astronautical Science and Mechanics, Harbin Institute of Technology (HIT), No. 92 West Dazhi Street, PO Box 301, Harbin 150001, PR China
[b] Center for Composite Materials and Structures, Harbin Institute of Technology (HIT), No. 2 YiKuang Street, Harbin, 150080, PR China

ARTICLE INFO

Keywords:
3D printing
Critical bistability
Variable cross-section
TENGs
PINN

ABSTRACT

Conventional damping materials face clear limitations in sports protection and rehabilitation. Their mechanical response is fixed and cannot adapt to varying impact intensities, and their lack of real-time monitoring prevents early identification of injury risks. To address these challenges, this study presents a fully printed intelligent shock-absorbing insole. The insole is fabricated using high-resolution 3D printing to construct a variable cross-section critical bistable structure, while all sensing and signal-processing circuits are produced with a circuit printer, enabling seamless integration without traditional wiring. The multilayer bistable architecture provides high energy absorption and rapid structural recovery, ensuring reusability. Distributed triboelectric nanogenerators (TENGs) embedded in the printed structure harvest mechanical energy during walking, forming a self-powered sensing system. A physics-informed neural network (PINN) is employed to identify impact force magnitude and location in real time, and a long short-term memory (LSTM) network processes gait sequences for dynamic injury-risk evaluation with an accuracy of 96.67%. Experiments demonstrate that the printed bistable structure achieves over 90% energy absorption efficiency under walking impacts, and the harvested energy is sufficient to drive the sensing module. This work integrates adaptive shock absorption, gait monitoring, and sustainable energy harvesting, offering a new paradigm for next-generation wearable devices in sports protection and rehabilitation medicine.

1. Introduction

In recent years, the advancement of wearable technologies has been remarkable, particularly in the development of smart footwear aimed at health monitoring, injury prevention, and performance optimization [1–3]. Among these innovations, shock-absorbing soles have drawn significant attention due to their potential to mitigate impact forces during physical activities, thereby reducing the risk of musculoskeletal injuries [4,5]. However, traditional shock-absorbing materials face inherent limitations: they cannot dynamically adapt to varying impact intensities and generally fail to provide real-time monitoring of the forces exerted on the foot [6,7]. This shortcoming underscores the pressing need for new approaches that integrate efficient energy absorption with advanced sensing and monitoring capabilities [8,9].

Bistable structures, which can exist in two stable equilibrium states, have been widely studied in mechanical engineering and materials science due to their unique energy storage capacity, memory effect, and nonlinear mechanical behavior [10–12]. Their advantages of structural simplicity, low cost, and high reliability make them attractive in applications such as mechanical switches and energy harvesting [13–16], with established uses in aerospace, robotics, and sensing systems [17,18]. Recent progress in additive manufacturing has further expanded the design space for bistable structures, enabling the fabrication of complex geometries and improving their functional performance [19,20]. However, conventional bistable structures still suffer from limited controllability, as they cannot actively and efficiently transition between stable states, thereby restricting their broader applicability.

To overcome these challenges, this paper proposes a novel shock-absorbing sole based on a multi-layered variable cross-section critical bistable structure integrated with triboelectric nanogenerators (TENGs). Through optimized geometric parameter design, the structure not only preserves the superior damping and energy absorption properties of bistable systems but also achieves enhanced recovery performance and reusability [21–23]. By embedding distributed TENG units, the system enables real-time monitoring of impact forces: each impact generates

* Corresponding authors.
E-mail addresses: zhaowei_2022@163.com (W. Zhao), yj_liu@hit.edu.cn (Y. Liu).

https://doi.org/10.1016/j.cej.2026.175093
Received 23 November 2025; Received in revised form 22 February 2026; Accepted 9 March 2026
Available online 9 March 2026

triboelectric signals that are processed by a neural network to determine the magnitude, direction, and distribution of the applied force. Deep learning algorithms further analyze the signals for gait recognition, providing continuous feedback on movement patterns and injury risks [32–34]. Importantly, the triboelectric energy harvested during impacts is used to power the system itself, ensuring a fully self-sustained operation without external energy input [24–31].

Overall, this work makes three key contributions. First, it introduces a controllable bistable structure with tunable geometry, offering enhanced damping efficiency and adaptability to a wide range of impact intensities. Second, it integrates TENG-based real-time force monitoring and gait analysis into the sole, providing advanced sensing and feedback functions. Third, it demonstrates a sustainable, self-powered platform that eliminates the need for external power sources. Taken together, these contributions position the proposed smart sole (Fig. 1) as a groundbreaking solution for impact protection, gait monitoring, and next-generation wearable devices [35–38].

2. Topology design

A constrained one-dimensional beam/truss structure is generally considered the simplest bistable unit [39], as shown in S.1a. The bistable behavior of this structure is primarily determined by its geometric configuration. By arranging and combining such structures in an array, multistable structures can be obtained, as illustrated in the figure. The multistable performance of these structures originates from the bistable units that compose them. This paper, therefore, introduces a novel variable cross-section multistable structure, which does not rely solely on the bistable capabilities of its components. Instead, bistability is achieved by adjusting the slope of the structure itself, without requiring each component to inherently possess bistable behavior.

2.1. Variable cross-section structure

For a one-dimensional beam structure, an adjustable bistable structure can be achieved by altering the geometric dimensions of the structure. For a bending beam structure with a section ratio $Q = H/T$, when Q is relatively small($Q < 1.23$), it behaves as a stable monostable structure. As the Q increases ($1.23 < Q < 2.31$), the structure transitions from a simple monostable state to a monostable state with sudden jumps. Finally, when the Q exceeds a certain threshold ($Q > 2.31$), the structure transforms into a fully bistable configuration, that is [40],

$$Q = \frac{H}{T} \text{with} \begin{cases} Q > Q_{cr} = 2.31 & \text{(bistability)} \\ 2.31 > Q > 1.23 & \text{(monostability with snap through)} \\ 1.23 > Q & \text{(simple stability)} \end{cases} \tag{1}$$

However, this paper demonstrates that when such a simple beam structure is combined into a special variable cross-section structure, the tower, composed of ordinary monostable one-dimensional beams, can exhibit snap-through or bistable behavior, as shown in Fig. 2b.

Based on this theory, the researchers designed a one-dimensional beam structure with a cosine-shaped curve (S.1b). Using the finite element method, a more detailed study was conducted on the section ratio $Q = H/T$, with additional research on the aspect ratio $R = L/H$. S.1cde presents the force-displacement curves of one-dimensional beam structures with different values of R and Q when the height is 10 mm. The researchers found that when the Q is large and the R is small, the slope of the force-displacement curve is more gradual, resulting in lower stiffness, with a segment that exhibits a platform region where the stiffness is approximately zero. Conversely, when the Q is small and the R is large, the slope of the force-displacement curve is steeper, and the stiffness is higher. Fig. 2a shows the corresponding force-displacement curves obtained from compression tests of one-dimensional beam structures with different R and Q when the height is 10 mm, which also validates the accuracy of the finite element analysis.

Particularly, as shown in Fig. 2b, when the aforementioned unit cells are assembled into a variable cross-section configuration, the originally non-bistable unit cells can exhibit bistable behavior. This bistable characteristic is significantly influenced by the structural inclination rate, geometric shape, and material properties. Research indicates that increasing the number of polygon sides in the variable cross-section structure enhances its bistable characteristics. Furthermore, reducing the structural inclination rate strengthens this bistable tendency. Simultaneously, a higher Young's modulus in the material also promotes bistable behavior. Based on these findings, researchers have demonstrated that by precisely controlling the geometric parameters of the structure, it is possible to achieve a critical state approaching bistability.

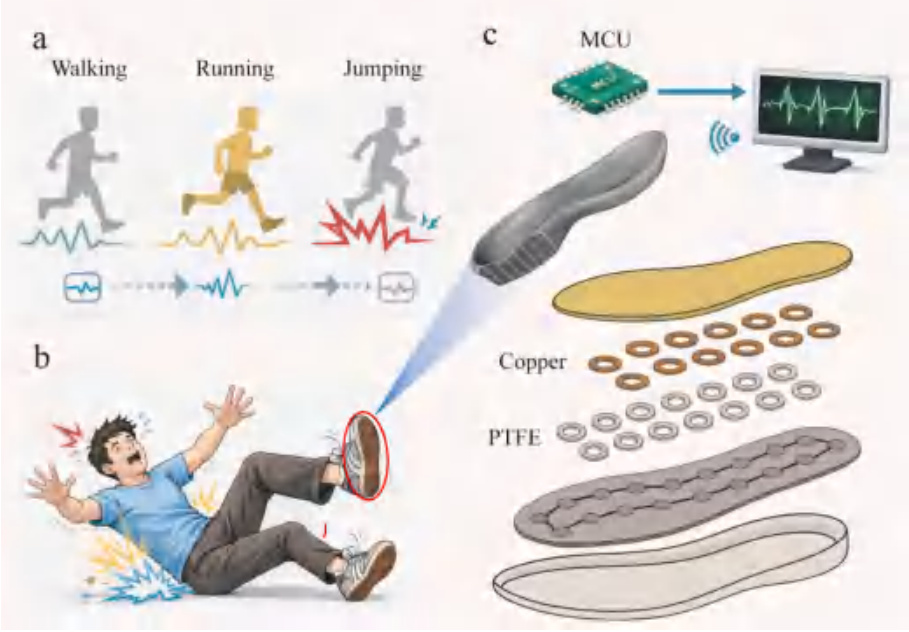

Fig. 1. Schematic of the self-powered smart sole system. (a) Representative gaits and signal acquisition. (b) Fall detection alert. (c) Exploded structure. (AI-assisted tools were used only at the stage of draft illustration/layout).

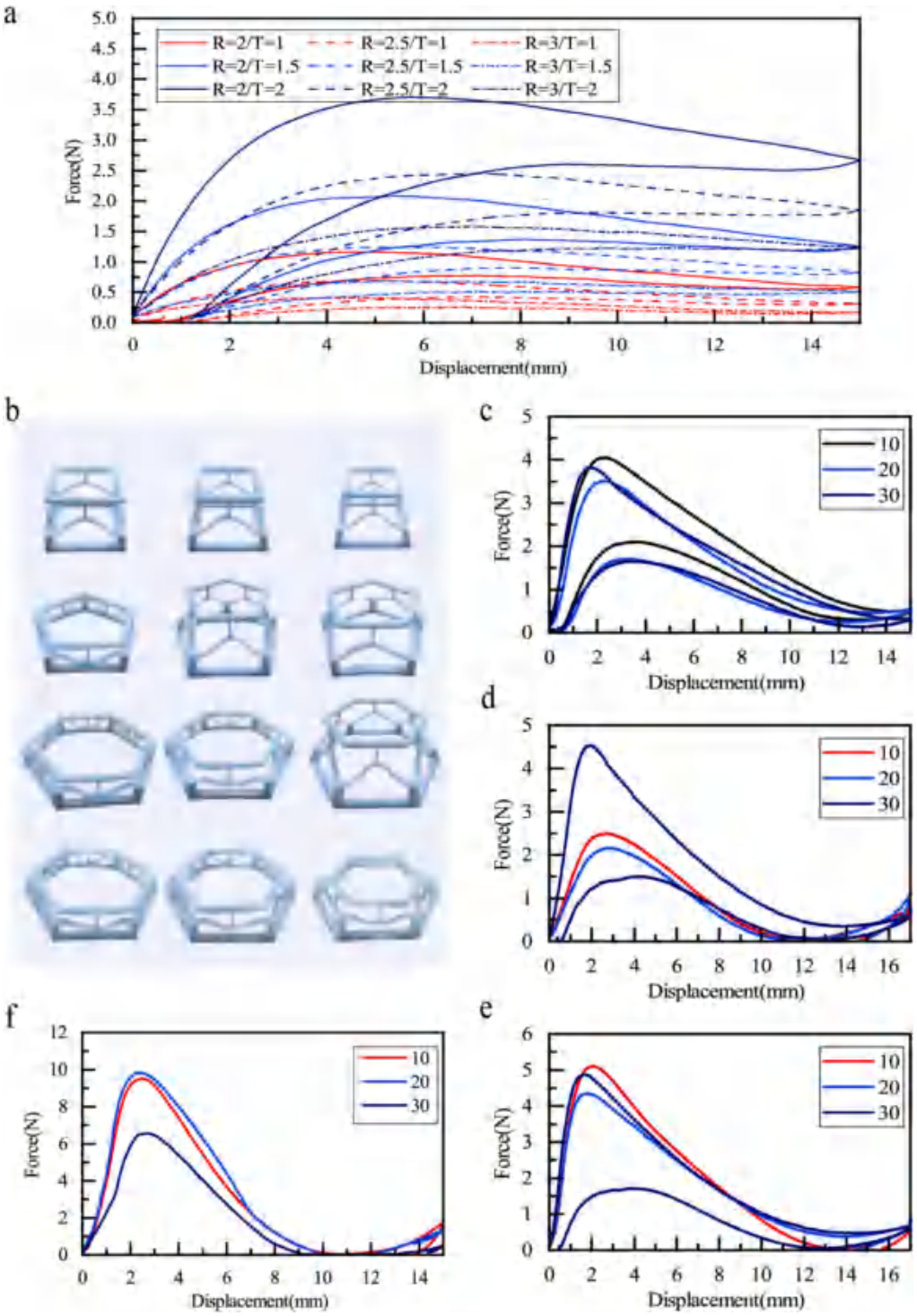

Fig. 2. Mechanical Analysis of the Unit Cell. (a) Compression test results of the unit cell. (b) variable cross-section structure with different topological designs. (c, d, e, f) Cyclic compression tests of variable cross-section structure with different topological designs.

This design preserves the excellent energy absorption and damping performance inherent to traditional bistable structures. Furthermore, it overcomes a critical technical limitation: the inability of such structures to achieve active switching between stable states. Consequently, structural reusability is significantly enhanced.

As shown in Fig. 2c-f, as the number of sides of the polygon increases, the bistable characteristics of the structure become more significant. Based on this finding, the circular structure was ultimately selected as the research object, with static compression experiments conducted at three inclination angles (10°, 20°, and 30°), supplemented by finite element simulation analysis. The material modulus in the finite element simulation is obtained from experiments(S. 2). As shown in Figure S. 3, the agreement between the finite element simulation results and the experimental data reaches more than 87%, indicating good prediction accuracy. In S.3c, F_d and F_{dF}represent the minimum force values obtained from experimental measurements and finite element simulations, respectively. When this value is zero, it indicates that the structure exhibits bistable characteristics at that inclination angle. $x_d$and

x_{dF}correspond to the displacement values at which the minimum force occurs in the experiment and finite element simulation, respectively.

The experiment shows the results of the finite element simulation, with specific data comparisons detailed in Table 1. It can be seen from the data in Table 1 that the bistable critical angle of the structure is between 22° and 23°. To ensure that the structure has an active recovery capability, its inclination angle is finally designed to be 23°.

2.2. Variable cross-section critical multistable structure

By stacking the aforementioned variable cross-section structures along the height direction, a tower-shaped critical multistable structure can be constructed. This structure exhibits three distinct load peaks during force application. Research demonstrates that by adjusting the thickness of the bending beams at each layer, the magnitude of each peak load can be precisely controlled. Fig. 3c presents the cyclic compression test results of a tower-shaped critical multistable structure with layer thicknesses of 1 mm, 2 mm, and 3 mm, respectively, corresponding to load peaks of 3.21 N, 5.50 N, and 9.58 N. Fig. 3d illustrates the performance of a uniform structure with identical layer thicknesses of 2 mm in cyclic compression tests, showing load peaks of 4.49 N, 4.93 N, and 5.95 N. Experimental results indicate that this structure exhibits excellent damping performance and energy absorption characteristics. Specifically, the structure in Fig. 3c demonstrates an energy absorption of 93.04 μJ with an energy absorption efficiency of 43.5%, while the structure in Fig. 4d shows an energy absorption of 70.70 μJ with an efficiency of 46.3%.

For sports shoe soles, the energy absorption rate is a vital performance metric. Higher absorption rates provide better protection for the human body during movement. Accordingly, we conducted drop-weight impact tests on our structure following the ASTM F1614–99 standard, using three impact energy levels (3 J, 5 J, 7 J) representing different motion states. To ensure experimental rigor, we established a control group (S.4a). Apart from structural differences, the test and control groups maintained identical size, mass, and material composition. The results are shown in Fig. 3e and f. The test group demonstrated energy absorption rates of 90.3%, 86.6%, and 83.4% under 3 J, 5 J, and 7 J impacts, respectively, significantly outperforming the control group's 74.3%, 71.6%, and 68% (S.4b). These results conclusively validate the superior energy absorption capabilities of the proposed structure.

2.3. Triboelectric nanogenerator

TENG is a novel energy-harvesting device based on the coupling effect of contact electrification and electrostatic induction. Its working principle primarily relies on the triboelectric charges generated when two different materials come into contact and separate, achieving electrical energy output through periodic mechanical motion. Research shows that the output performance of TENGs is mainly influenced by factors such as surface charge density, contact area, applied pressure, and operating frequency. By optimizing the selection of triboelectric materials, surface microstructure design, and circuit matching, the energy conversion efficiency of TENGs can be significantly improved. Currently, TENGs demonstrate broad application prospects in self-powered sensors, wearable devices, and environmental energy harvesting.

This study innovatively integrates the triboelectric effect with structural design, as shown in Fig. 4a, enabling the structure to simultaneously achieve vibration damping and energy absorption while effectively harvesting mechanical energy from impacts and converting it into electrical energy. The triboelectric generation module adopts a five-layer composite structure design: the upper part consists of a fixed layer, a conductive layer, and a polytetrafluoroethylene (PTFE) layer, while the lower part comprises a copper foil layer and a fixed layer. The periodic contact and separation between the PTFE layer and copper foil layer generate triboelectric charges. The fixed layer not only provides structural support but also enhances the triboelectric effect between PTFE and copper foil through its elastic properties. The conductive layer is responsible for collecting the electrostatic charges generated on the PTFE surface.

The current and voltage response characteristics of the device under different impact frequencies and amplitudes are shown in Fig. 4b-e. The results demonstrate that as the impact frequency and amplitude increase, the output current and voltage of the device show growth trends. To evaluate the electrical output performance of the device, we connected it as a power source to a test circuit and investigated the influence of external load impedance on the output characteristics. Experimental data indicate that the device reaches its maximum output power of 12.89 μW when the load impedance is approximately 10 MΩ (Fig. 4f).

Furthermore, a numerical model established via COMSOL Multiphysics software successfully simulated the dynamic potential distribution during the contact-separation process (Fig. 4 g). The simulation results reveal the potential evolution law of the dual electrodes during the charge transfer process. Durability tests show (S. 5) that after 10,000 cycles of impact, the output voltage stability of the device remains above 97.3% of the initial value, indicating that it has excellent mechanical reliability and output stability.

3. Impact recognition during motion

Motion impact recognition is a critical technology aimed at real-time detection and analysis of transient impact events occurring during motion. This paper employs embedded devices to capture dynamic signals during motion and combines machine learning algorithms to achieve intelligent classification and localization of impact patterns. In practical applications, motion impact recognition technology holds significant value in areas such as sports injury prevention, athletic performance analysis, and the development of intelligent sports equipment.

3.1. Embedded device design

To achieve real-time and rapid acquisition of electrical signals generated by impacts, researchers have developed an embedded electrical signal acquisition system (Fig. 5a and b). The core control unit of this system employs the F103C8T6 microcontroller from STMicroelectronics' STM32 series, known for its high performance and low power consumption. To meet the requirements of multi-channel signal acquisition, the system utilizes the GPIO expansion chip MCP23017 to achieve synchronous acquisition of electrical signals from multiple triboelectric generators and measures the triboelectric voltage via the ADC module. The specific circuit is shown in S. 7. The system incorporates optimized data acquisition algorithms and efficient signal transmission protocols, achieving microsecond-level temporal resolution, which ensures the real-time capability and accuracy of impact signal detection. Experimental results confirm that the system maintains a high sampling rate of up to 1 MHz/s. Furthermore, it demonstrates excellent signal fidelity and robust anti-interference capabilities. These combined attributes provide reliable data for subsequent impact

Table 1
Finite element simulation force-displacement curves of critical bistable structures under different inclination angles.

Degree(°)	10	15	19	20	21	22	23	25	30
x_{dF}(mm)	11.25	11.67	12.04	12.53	14.15	15.87	17	17	17
F_{dF}(N)	0	0	0	0	0	0	0.12	0.34	0.74

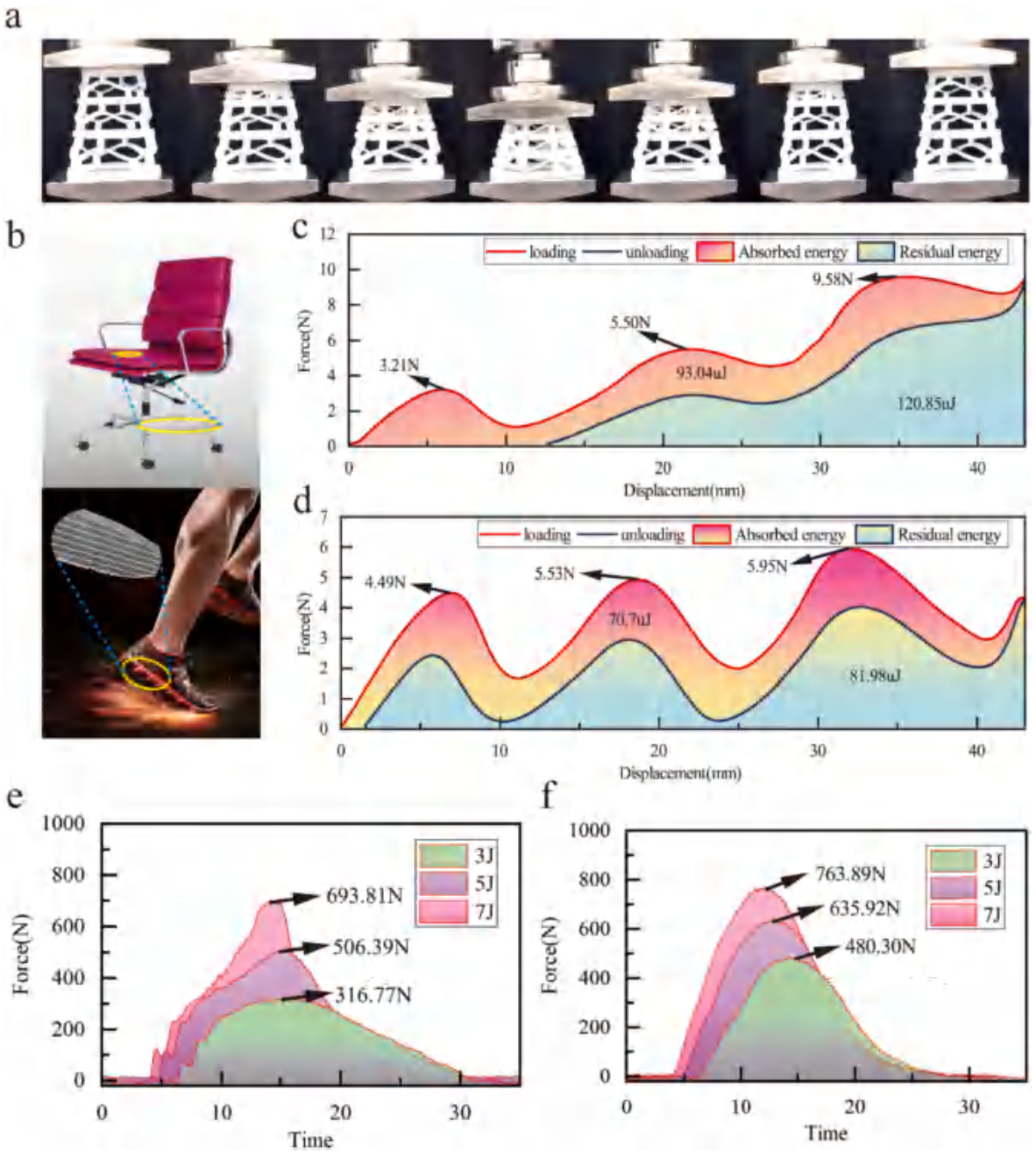

Fig. 3. Variable cross-section critical multistable structure. (a) Compression test of the variable cross-section critical multistable structure. (b) Possible application scenarios for this structure. (c) Force-displacement curve under cyclic compression with different layer thicknesses. (d) Force-displacement curve under cyclic compression with different layer thicknesses.

characteristic analysis and energy harvesting research.

3.2. Physics-informed neural network (PINN)

Physics-Informed Neural Networks (PINN) represent a novel deep learning framework that embeds physical laws into neural network architectures [41]. This approach achieves an organic integration of data-driven methods and physical principles by incorporating physical constraints such as governing equations, boundary conditions, and initial conditions into the loss function as soft constraints. The core feature of PINN lies in its unique loss function design, which typically consists of two components: a data-fitting term and a physics-constrained term. The data-fitting term ensures consistency between network outputs and experimental or observational data, while the physics-constrained term guarantees that the solutions satisfy the given physical laws.

In a space equipped with triboelectric generators, this study constructs a Physics-Informed Neural Network (PINN) model for impact event prediction and localization. The PINN model takes the voltage signal v and spatial position x as inputs and outputs the impact force magnitude F and impact location X. Here, the voltage signal v is collected by the triboelectric devices, and the spatial position x corresponds to the sensor deployment coordinates. The loss function of this model consists of a data-fitting term and a physics-constrained term (Fig. 5c):

$$Loss_{total} = \omega Loss_{data} + (1-\omega) Loss_{physics} \quad (2)$$

where,

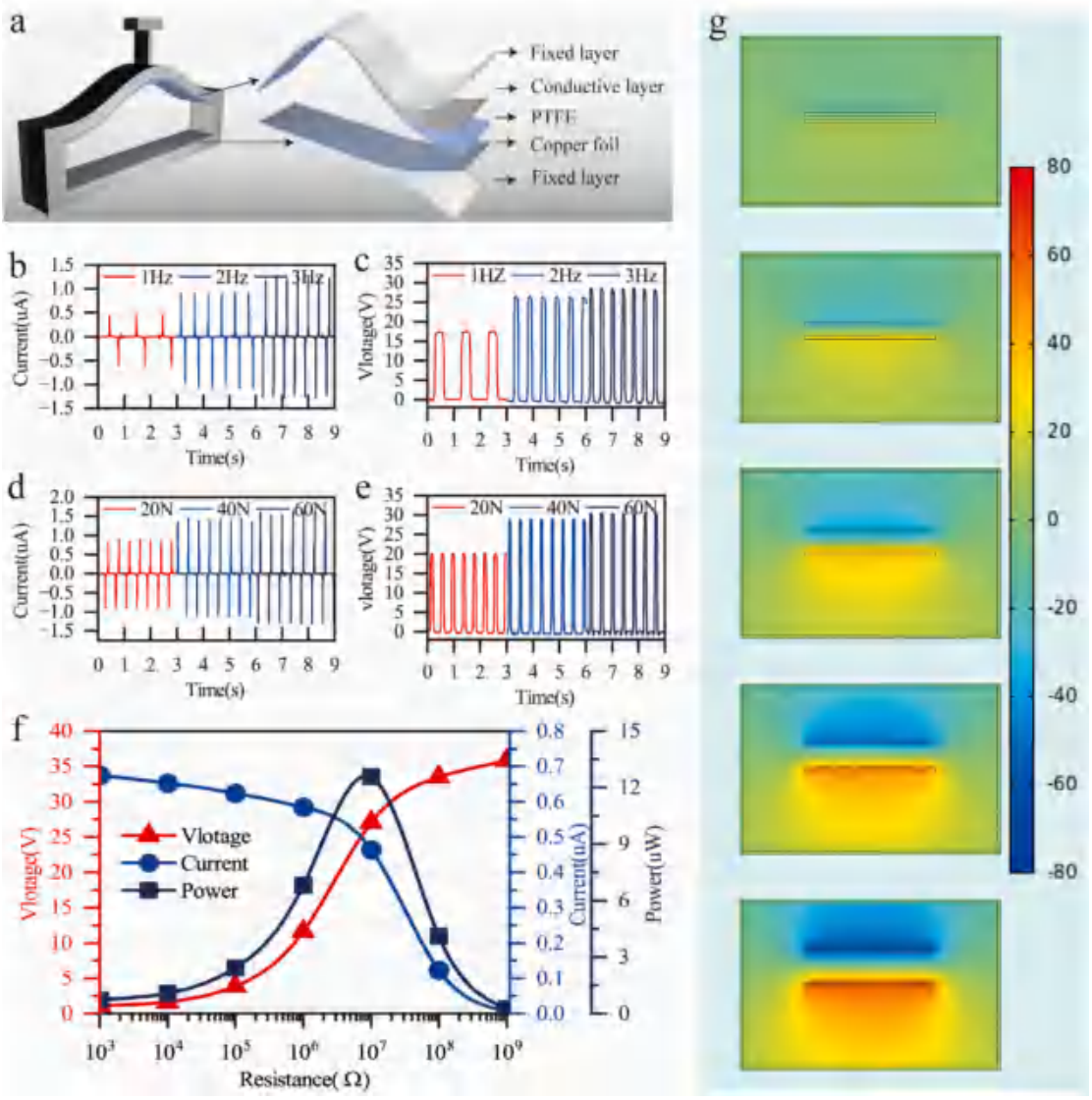

Fig. 4. triboelectric nanogenerator. (a) Schematic diagram of the structure of a triboelectric nanogenerator. (b, c) Voltage and current diagrams under impact at different frequencies. (d, e) Voltage and current diagrams under impact at different forces. (f) Output Power as a Function of Load Impedance. (g) Electric Potential Diagram of a Triboelectric Nanogenerator Simulated Using COMSOL Software.

$$Loss_{data} = \frac{1}{N_F}\sum_{i}^{N_F}\left|F(x^i_{data}, v^i_{data}) - F^i_{data}\right|^2 + \frac{1}{N_X}\sum_{i}^{N_X}\left|X(x^i_{data}, v^i_{data}) - X^i_{data}\right|^2 \tag{3}$$

$$Loss_{physics} = Loss_F + Loss_X \tag{4}$$

The data-fitting term $Loss_{data}$ ensures consistency between network outputs and experimental observations, while the physics-constrained term $Loss_{physics}$ incorporates mechanical principles to guarantee the physical plausibility of predictions. Here ω is the loss function factor. When $\omega = 1$the model is purely data-driven, when $\omega = 0$, the model is entirely driven by physical constraints. This PINN design utilizes limited experimental data for effective training. Furthermore, it improves prediction accuracy by incorporating physical law constraints. The approach demonstrates excellent generalization capabilities, particularly in data-sparse regions.

The physical formula for the impact location and magnitude is

$$F = \sum_{i=1}^{N_x}\lambda\cdot v\cdot\chi(x), \quad X = \frac{\sum_{i=1}^{N_x}\lambda\cdot vx\cdot\chi(x)}{\sum_{i=1}^{N_x}x\cdot\chi(x)} \tag{5}$$

where, $\lambda$is a hyperparameter (S. 13), and$\chi(x)$is the electric signal distribution function. When a triboelectric generator at the coordinate$x_i$generates an electric signal, $\chi(x_i) = 1$otherwise $\chi(x_i) = 0$.

According to Eq.(5), the physical loss function was constructed as

$$Loss_{physics} = \frac{1}{n}\sum_{i=1}^{n}\left|\frac{\widehat{F}_i - F_i}{F_i}\right|^2 + \left|\frac{\widehat{X}_i - X_i}{X_i}\right|^2 \tag{6}$$

where n is the number of samples. $\widehat{F}_i$ and F_i are the predicted and the expected Force of the i-th sample, $\widehat{X}_i$ and X_i are the predicted and the expected position of the i-th sample.

To validate the prediction accuracy of the model, the researchers constructed a test dataset containing 15 samples. As shown in S. 8, the visualization results compare the spatial distribution of the actual impact position with the model's predictions. S. 9 displays the

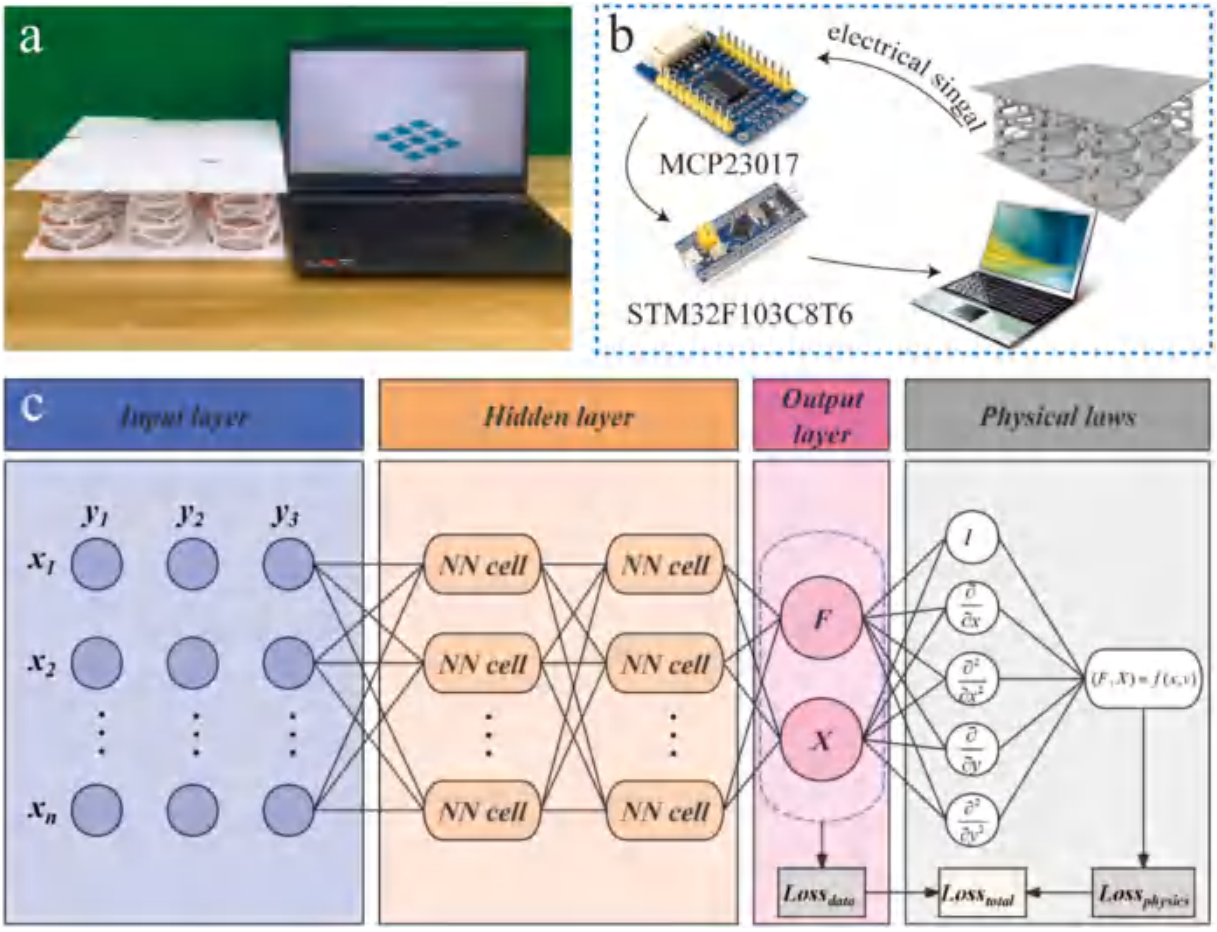

Fig. 5. Physics-Informed Neural Network (PINN). (a, b) The physical schematic and diagram of the load identification system. (c) Schematic diagram of the PINN. (d) Comparison of predicted force and position with the actual force and position. (e) MAE and MSE change with the increase in training epochs.

convergence curves of the mean absolute error (MAE) during the model training process. The experimental results demonstrate that the constructed PINN model achieves a prediction accuracy of 92.3% on the test set, fully confirming the model's effectiveness in predicting impact force and position. It is noteworthy that the prediction errors are primarily concentrated in small-scale impact events, which may be attributed to the weaker electrical signals generated by small-scale impacts, thereby increasing the difficulty of feature extraction.

4. Results and discussion

Based on the preceding research, a variable cross-section multi-stable structure with superior shock absorption and energy dissipation properties was developed. By leveraging triboelectric nanogenerator (TENG) signals distributed across this structure and employing neural network training, structural impacts can be monitored. This foundation enabled the fabrication of an energy-dissipating sole with integrated motion gait monitoring capabilities.

4.1. Soles unit cell distribution design

During motion, the pressure in the sole region undergoes periodic changes (Fig. 6a). Based on this data, the unit cells at different positions of the soles are adjusted, the thickness T of the curved beams of the unit cells is modulated according to the pressure in different regions (S. 14). This ensures that the insole is stiffer in areas with higher pressure to provide adequate support, while being softer in areas with lower pressure to protect the foot and offer a more comfortable wearing experience.

4.2. Shock absorption performance of the insole

To evaluate the shock absorption performance of the soles, we conducted plantar pressure experiments with testers both barefoot and wearing the smart soles. To obtain accurate data, the testers were first allowed to move for 20 s to stabilize their gait, after which the average and maximum plantar pressures under different motion states were recorded (Fig. 6b and c).

In the barefoot walking state, the average plantar pressure was 531.68 g/cm^2, and the maximum pressure was 884.35 g/cm^2. When wearing the soles during walking, the average plantar pressure was 334.56 g/cm^2, and the maximum pressure was 548.12 g/cm^2.In the barefoot running state, the average plantar pressure was 723.83 g/cm^2, and the maximum pressure was 1224.75 g/cm^2. When wearing the soles during running, the average plantar pressure was 391.26 g/cm^2, and the maximum pressure was 634.23 g/cm^2. When wearing the smart soles during walking, the average plantar pressure was reduced by 37.07%, and the maximum pressure was reduced by 38.02%. During running, the average plantar pressure was reduced by 45.94%, and the maximum pressure was reduced by 48.21%. This significantly mitigates the impact on the human body during motion, ensuring the safety of users. The corresponding plantar pressure distribution is illustrated in Fig. 6d.

It is noteworthy that at slower speeds, the maximum pressure curve forms a distinct plateau region. As the speed increases, this plateau region gradually diminishes until it forms a sharp peak. This characteristic is particularly suitable for data collection using deep learning models.

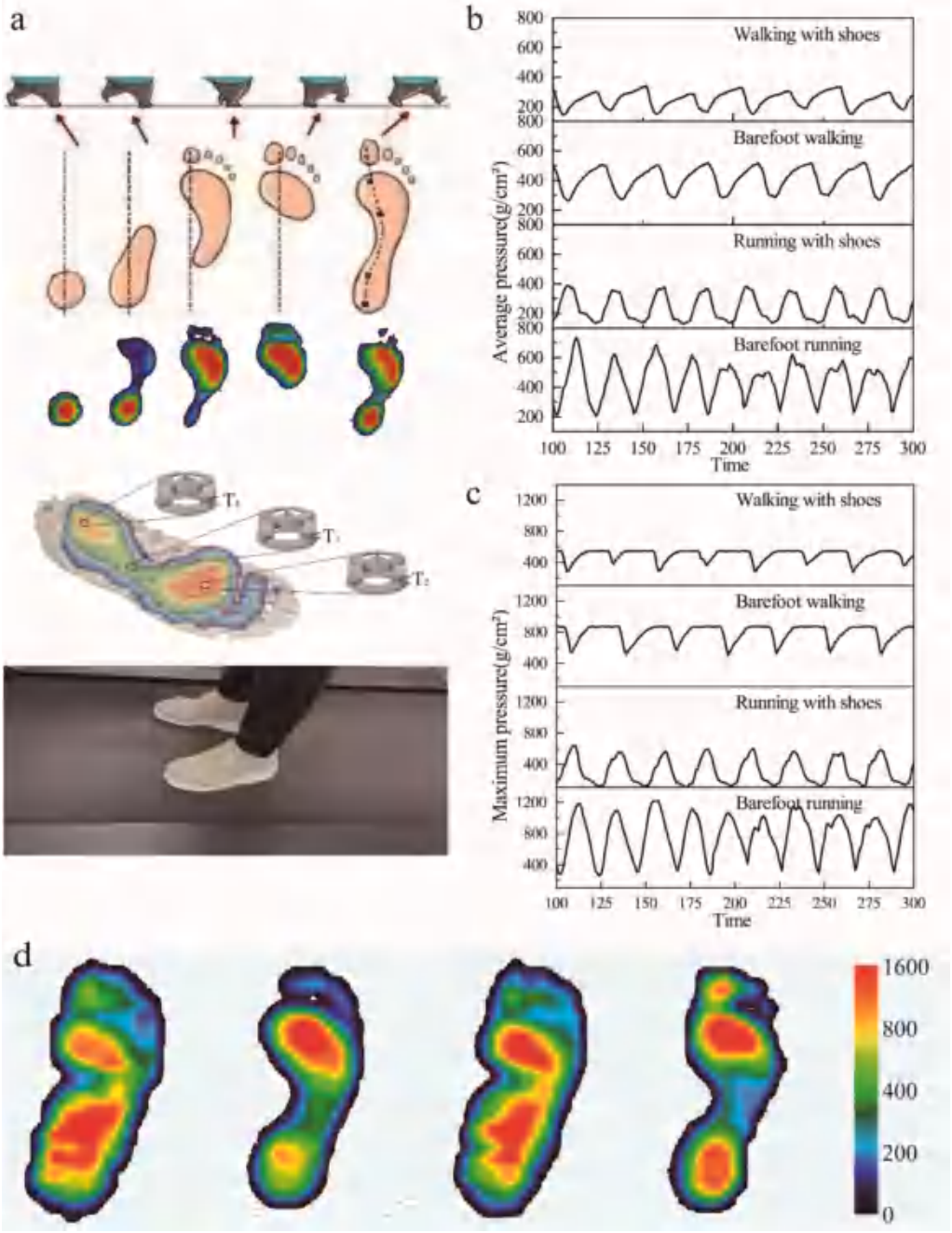

Fig. 6. Fabrication and Performance of Smart Soles. (a) Plantar pressure dynamics during a motion cycle and Corresponding single-cell soles design strategy, with a physical demonstration of the designed footwear worn by test subjects (b, c) Average pressure and maximum pressure in the sole region with and without the soles under different motion states. (d) Plantar pressure distribution map under different conditions.

Therefore, in this study, based on the foot pressure distribution predicted by the PINN network in the previous section, this distribution is used as input along with the electrical signals to determine the wearer's gait.

To capture both temporal and spatial information, a combination of 1D CNN and LSTM models is employed to process the data. The overall model structure is illustrated in Fig. 7b, and the electrical signals collected under different motion states are shown in Fig. 7c. Finally, the prediction results for six different gaits from nine volunteers are presented in Fig. 7d, achieving an overall accuracy of 99.6%.

However, it can be observed that as the intensity of the motion increases, the prediction accuracy decreases. This may be due to the more chaotic data generated during intense motion, making it harder to capture meaningful patterns. Additionally, when the motion reaches a certain level of intensity, the electrical output of some triboelectric generators may saturate, no longer increasing. This saturation could also potentially affect the prediction accuracy.

5. Conclusion

This paper proposes novel smart shock-absorbing soles. The design integrates a variable cross-section multistable structure with triboelectric nanogenerators (TENGs). This integration addresses two limitations of traditional damping materials. First, conventional materials cannot dynamically adapt to varying impact intensities. Second, they lack real-time monitoring capabilities. Through geometric parameter

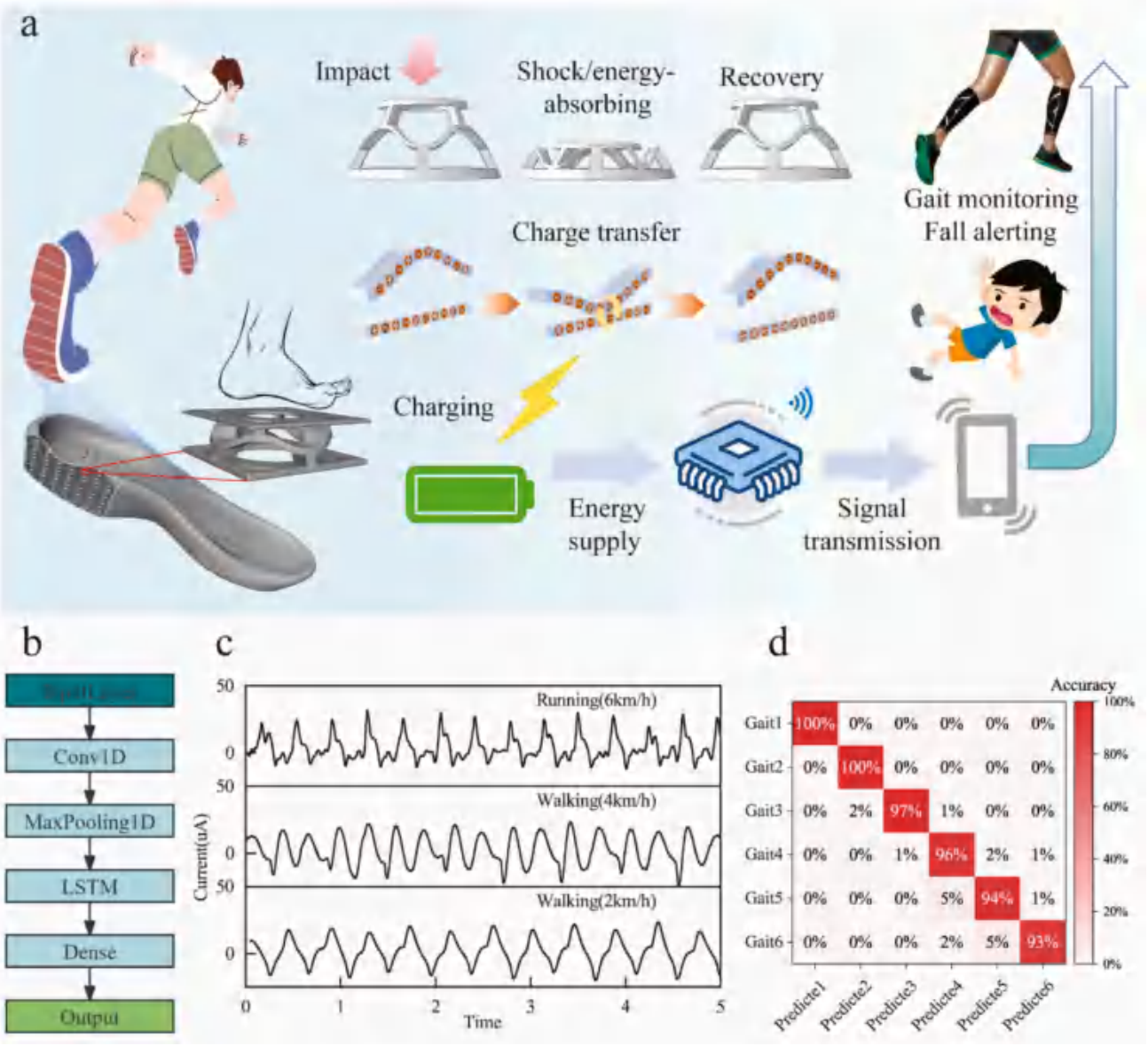

Fig. 7. Gait Monitoring Workflow. (a) Schematic Diagram of the Soles Working Principle. (b) Schematic diagram of the neural network for gait recognition. (c) Electrical signals are generated by the soles under different motion states. (d) Confusion matrix of prediction results for six common gaits.

optimization, the critical structure retains the superior energy absorption and damping properties of conventional bistable designs while significantly enhancing structural recovery performance and reusability. A key innovation lies in embedding distributed TENG units within the soles. These convert mechanical energy into electricity via contact-separation effects. When processed by deep learning algorithms, the generated signals enable real-time monitoring of impact force magnitude (±8% accuracy) and spatial position. This integrated system achieves high-precision motion gait tracking. Synchronously collected gait data, processed by LSTM networks, enables dynamic assessment of sports injury risks (recognition accuracy 96.67%). Experimental results demonstrate that the multi-layer critical bistable structure exhibits excellent shock absorption and energy dissipation capabilities under impact loads generated during normal human walking. The self-powered system generates sufficient triboelectric energy during normal walking to meet the energy requirements of the sensing module. This technology integrates advanced material design, intelligent sensing, and energy harvesting, establishing an innovative paradigm for wearable devices in sports protection and rehabilitation medicine, offering adaptive shock absorption, biomechanical monitoring, and sustainable power supply capabilities. Future research could further optimize geometric parameters and material selection to enhance the structure's energy absorption and damping performance. Additionally, more application scenarios, such as medical rehabilitation and sports training, could be explored to further validate the practicality and reliability of this technology. Furthermore, the research could focus on improving the energy conversion efficiency of TENGs to support more sensing and data processing functions.

CRediT authorship contribution statement

Jian Zhou: Writing – review & editing, Writing – original draft, Visualization, Validation, Software, Data curation. **Chengjun Zeng:** Visualization, Validation. **Wei Zhao:** Writing – review & editing, Visualization, Validation, Conceptualization. **Jinsong Leng:** Writing – review & editing, Visualization, Validation, Funding acquisition. **Yanju Liu:** Writing – review & editing, Visualization, Funding acquisition.

Declaration of competing interest

The authors declare that they have no known competing financial interests or personal relationships that could have appeared to influence the work reported in this paper.

Acknowledgments

This work is supported by the National Key Research and Development Program of China (2022YFB3805700, 2024YFB4710205), National Natural Science Foundation of China (Grant No. 12472147, U23A20412, 12402160) and Young Elite Scientists Sponsorship Program by CAST (Grant No. 2023QNRC001), Heilongjiang Provincial Natural Science Foundation of China 2022ZX02C25, Scientific Research Project of Heilongjiang Provincial Health Commission (Grant No. 20230808050140).

Appendix A. Supplementary data

Supplementary data to this article can be found online at https://doi.org/10.1016/j.cej.2026.175093.

Data availability

Data will be made available on request.

References

[1] I. Almuteb, R. Hua, Y. Wang, Smart insoles review (2008-2021): applications, potentials, and future, Smart Health 25 (2022) 100301.
[2] P.G. Rukmini, R.B. Hegde, B.K. Basavarajappa, et al., Recent innovations in footwear and the role of smart footwear in healthcare—a survey, Sensors 24 (13) (2024) 4301.
[3] Yu Binhai, Zijian Huang, Yu Shudong, et al., Biomimetic porous fluoropolymer films with brilliant whiteness by using polymerization-induced phase separation, Adv. Mater. Interfaces 9 (1) (2022) 2101485.
[4] W.S. Singh, N. Srilatha, Design and analysis of shock absorber: a review, Mater. Today Proc. 5 (2) (2018) 4832–4837.
[5] M. Corsi, S. Bagassi, M.C. Moruzzi, et al., Additively manufactured negative stiffness structures for shock absorber applications, Mech. Adv. Mater. Struct. 29 (7) (2022) 999–1010.
[6] S.K. Sung, H.J. Yoon, S.W. Kim, Textile-based triboelectric nanogenerators for self-powered wearable electronics, Adv. Funct. Mater. 29 (2) (2019) 1804533.
[7] J.P. Wu, X.R. Teng, L. Liu, et al., Eutectogel-based self-powered wearable sensor for health monitoring in harsh environments, Nano Res. 17 (6) (2024) 5559–5568.
[8] Z.L. Wang, Triboelectric nanogenerator (TENG)—sparking an energy and sensor revolution, Adv. Energy Mater. 10 (17) (2020) 2000137.
[9] X.J. Li, C.M. Jiang, F.N. Zhao, et al., Fully stretchable triboelectric nanogenerator for energy harvesting and self-powered sensing, Nano Energy 61 (2019) 78–85.
[10] E. Ammar, Bistable morphing composites for energy-harvesting applications, Polymers 14 (9) (2022) 1893.
[11] C. Sarit, S.K. Mandal. Magnetoelectric Zn0. 2Co0. 8Fe2O4-PbZr0. 58Ti0. 42O3 nanocomposite for bistable memory and magnetic field sensor applications. J. Magn. Magn. Mater., 2019, 491: 165573.
[12] S. Chiacchiari, F. Romeo, M.D. McFarland, et al., Vibration energy harvesting from impulsive excitations via a bistable nonlinear attachment experimental study, Mech. Syst. Signal Process. 125 (2019) 185–201.
[13] W.Q. Liu, F. Formosa, A. Badel, et al., Self-powered nonlinear harvesting circuit with a mechanical switch structure for a bistable generator with stoppers, Sensors Actuators A Phys. 216 (2014) 106–115.
[14] G.D. Pietro, G. Giunta, Y. Hui, et al., A novel computational framework for the analysis of bistable composite beam structures, Compos. Struct. 257 (2021) 113167.
[15] D. Tenenbaum, J.I. Marrone, E. Hernán, et al., Robustness in spatially driven bistability in signaling systems, Sci. Rep. 10 (1) (2020) 5591.
[16] X. Chao, H. Hu, J. Lin, et al., Bioinspired twist-hyperbolic metamaterial for impact buffering and self-powered real-time sensing in UAVs. Science, Advances 11 (36) (2025) eadw6179.
[17] K. Zouhri, M. Mohamed, A. Erol, et al., Innovative Bistable composites for aerospace and high-stress applications: integrating soft and hard materials in experimental, modeling, and simulation studies, Materials 17 (17) (2024) 4280.
[18] J.X. Zhu, X.M. Liu, Q.F. Shi, et al., Development trends and perspectives of future sensors and MEMS/NEMS, Micromachines 11 (1) (2019) 7.
[19] Y.T. Cao, M. Derakhshani, Y.H. Fang, et al., Bistable structures for advanced functional systems, Adv. Funct. Mater. 31 (45) (2021) 2106231.
[20] Y. Choi, G. Morlino, A. Toboso-Navasa, et al., A novel bistable device to study mechanosensitive cell responses to instantaneous stretch, Biomater. Adv. 141 (2022) 213134.
[21] Y.G. Leng, T.Y. Wang, Y. Guo, et al., Engineering signal processing based on bistable stochastic resonance, Mech. Syst. Signal Process. 21 (1) (2007) 138–150.
[22] H.L. He, T.Y. Wang, Y.G. Leng, et al., Study on non-linear filter characteristic and engineering application of cascaded bistable stochastic resonance system, Mech. Syst. Signal Process. 21 (7) (2007) 2740–2749.
[23] M.J. Yao, C.J. Zeng, J.S. Leng, et al., 4D printed cardiac occlusion device with efficient anticoagulation, Proendothelialization, and precise localization, Adv. Funct. Mater. 2412533 (2025).
[24] S.M.A. Iqbal, I. Mahgoub, E. Du, et al., Advances in healthcare wearable devices. NPJ flexible, Electronics 5 (2021) 9.
[25] S. Beniczky, P. Karoly, E. Nurse, et al., Machine learning and wearable devices of the future, Epilepsia 62 (2021) S116–S124.
[26] K. Rawy, R. Sharma, H.J. Yoon, et al., A triboelectric nanogenerator energy harvesting system based on load-aware control for input power from 2.4 μW to 15.6 μW, Nano Energy 74 (2020) 104839.
[27] S.M. Niu, Y.S. Zhou, S.H. Wang, et al., Simulation method for optimizing the performance of an integrated triboelectric nanogenerator energy harvesting system, Nano Energy 8 (2014) 150–156.
[28] S.M. Niu, Z.L. Wang, Theoretical systems of triboelectric nanogenerators, Nano Energy 14 (2015) 161–192.
[29] T.H. Chen, J.J. Shao, Z.L. Wang, Triboelectric nanogenerators, Nat. Rev. Methods Primers 1 (2023) 39.
[30] S. Parandeh, N. Etemadi, M. Kharaziha, et al., Advances in triboelectric nanogenerators for self-powered regenerative medicine, Adv. Funct. Mater. 47 (2021) 2105169.
[31] D. G. Dassanayaka, T. M. Alves, N. Wanasekara, et al. Recent progresses in wearable triboelectric nanogenerators. Adv. Funct. Mater., 2022, 32(44): 2205438.
[32] A.S. Alharthi, S.U. Yunas, K.B. Ozanyan, Deep learning for monitoring of human gait: a review, IEEE Sensors J. 21 (2019) 9575–9591.
[33] J.L. Chen, Y.N. Dai, N.S. Grimaldi, et al., Plantar pressure-based insole gait monitoring techniques for diseases monitoring and analysis: a review, Adv. Mater. Technol. 7 (1) (2022) 2100566.
[34] M. Canonico, F. Desimoni, A. Ferrero, et al. Gait monitoring and analysis: a mathematical approach. Sensors, 2023, 23(18): 7743.
[35] R.T. Li, S.R. Kling, M.J. Salata, et al., Wearable performance devices in sports medicine, Sports health 8 (1) (2016) 74–78.
[36] S. J. Park, I. Hussain, S. Hong, et al. Real-time gait monitoring system for consumer stroke prediction service. In: 2020 IEEE international conference on consumer electronics (ICCE). IEEE, 2020, 1–4.
[37] J. E. Wu, K. Kuruvithadam, A. Schaer, et al. An intelligent in-shoe system for gait monitoring and analysis with optimized sampling and real-time visualization capabilities. Sensors, 2021, 21(8): 2869.
[38] S. Seneviratne, Y. N. Hu, T. Nguyen, et al. A survey of wearable devices and challenges. IEEE Commun. Surv. Tutor., 2017, 19(4): 2573–2620.
[39] K. Liang, S. J. Zhou, Y. J. Luo, et al. Topology optimization design of recoverable bistable structures for energy absorption with embedded shape memory alloys. Thin-Walled Struct., 2024, 198: 111757.
[40] J. Qiu, J.H. Lang, A.H. Slocum, A curved-beam bistable mechanism, J. Microelectromech. Syst. 13 (2) (2004) 137–146.
[41] H. Hu, L. Qi, X. Chao, Physics-informed neural networks (PINN) for computational solid mechanics: numerical frameworks and applications, Thin-Walled Struct. 205 (2024) 112495.